Communication

Planar Triorthogonal Diversity Slot Antenna

Nicholas P. Lawrence, Christophe Fumeaux, and Derek Abbott

***Abstract*— This communication proposes an easily manufacturable multifunction multiport planar slot antenna with triorthogonal pattern diversity. Distinct radiation patterns are emitted via a common square radiative slot by exploiting three orthogonal modes. These slot modes consist of a magnetic current loop mode with an omnidirectional linearly polarized (OLP) radiation pattern, and two degenerated linear slot modes radiating broadside with orthogonal linear polarizations (LPs). The triorthogonal patterns are obtained in an overlapping frequency band, and the mutual coupling between the ports is minimized through a differential feeding arrangement. This new concept of multiport diversity slot antenna is validated experimentally at a frequency of 5.9 GHz, successfully demonstrating the operation modalities of OLP and LP radiation patterns. A minimum triorthogonal overlapping impedance bandwidth of 2.3% is measured with interport coupling below −35 dB. The proposed antenna could be used as a pattern and polarization diversity antenna, where additionally, a linear combination of the primary triorthogonal patterns can be exploited to further enhance flexibility in pattern generation.**

***Index Terms*— Multifunction, planar, polarization diversity, triorthogonal.**

I. Introduction

An increasing number of wireless communications technologies in the microwave region, and indeed beyond, are focused on driving up transmission rate. An increase in rate is often at the expense of coverage. The ability to send and receive signals in any direction without compromising link reliability would be highly desirable.

Using a single multiport antenna structure with pattern diversity and low mutual coupling between different ports is one possible solution toward higher link reliability in any direction. The available literature mostly focuses on multiport printed diversity antennas or planar inverted-F antennas (PIFA) due to their compactness, low cost, and low profile [1]–[3]. However, these antennas often suffer from a combination of a complicated structure, large size, poor radiation pattern symmetry, relatively low gain, and a little consideration of polarization orthogonal to the antenna surface.

The benefit of transmitting a second orthogonally polarized signal is well known [4], [5]. Polarization diversity offers performance robustness in a small volume, provided mutual coupling between polarizations [6] can be kept low, such as in an orthogonal system [7]. The robustness of dual-polarized systems is, however, adversely affected by transmitter–receiver misalignment.

To mitigate this problem and introduce orientation robustness in a rich scattering environment, the increase in capacity performance offered by colocated antennas in a triorthogonal arrangement has previously been highlighted [8]–[16]. Such systems demonstrate the benefit of a third orthogonal antenna, but realized configurations are typically large and impractical. To emit, three isolated and orthogonal polarizations from a small volume would be highly desirable for implementing reliable link performance in any direction.

A colocated triorthogonal antenna employing a dielectric resonator antenna as an integrated solution to generate three orthogonally polarized signals, including one parallel to the direction of propagation, has been demonstrated in [17], in a nonplanar solution. Monopoles placed at the center of a triorthogonal antenna add to design and implementation complexity requiring dual-substrate manufacture [18], [19]. A low profile triorthogonal design was presented in [20], however, with an asymmetric configuration creating a pattern asymmetry in the far field.

In contrast to previously proposed nonplanar triorthogonal designs, this communication proposes a multiport planar slot antenna capable of transmitting phase-centered polarized signals in three orthogonal directions, while providing high interport isolation due to a differential feeding technique. Two broadside patterns with orthogonal polarizations are generated by selective excitation of degenerated slot modes, whereas the third polarization, in the z-direction, is offered through the inclusion of a low-profile magnetic current loop electric monopole [21].

This communication provides first a generic description of the proposed concept of a multiport slot antenna with differential feeding. It then describes as illustration a specific design at a frequency of 5.9 GHz. A purpose-built feeding network is then combined with the antenna to experimentally demonstrate the performance in triorthogonal modes. In summary, the experimental results validate the concept, in particular with measured interport coupling coefficients below −35 dB.

II. Antenna Design and Feed Network

A. General Concept

The proposed design in Fig. 1 may be considered as a square slot antenna allowing three orthogonal polarized modes to radiate from the antenna upper surface. Fig. 2 shows the modes of operation in the antenna, namely, a magnetic current loop mode in Fig. 2(a), for omnidirectional linearly polarized (OLP) radiation, and two degenerated broadside dual-slot modes in Fig. 2(b) and (c), for orthogonal linear polarization (LP) radiation states. The radiative mechanism of the three modes through the common radiative square slot on the antenna upper surface, enabling triorthogonal polarization generation, is clearly shown.

We summarize an initial design procedure as follows.

1) *Magnetic Current Loop Mode:* When excited in its center, at port 0, the substrate-integrated geometry forms a square cavity, shorted to the intact metallized antenna backside ground plane using eight vias, two at each corner. The cavity walls, or rectangular apertures, between the shorting vias can be approximated as nearly perfect magnetic conductors (with radiation losses). The electric field in the apertures forms a subwavelength magnetic current loop, which radiates as an equivalent electric dipole. Consequently, this magnetic current loop mode of operation radiates a monopole pattern with vertical polarization orthogonal to the antenna surface [21].

Manuscript received March 23, 2016; revised December 6, 2016; accepted December 12, 2016. Date of publication January 4, 2017; date of current version March 1, 2017.

The authors are with the School of Electrical and Electronic Engineering, The University of Adelaide, Adelaide, SA 5005, Australia (e-mail: nicholas.lawrence@adelaide.edu.au; christophe.fumeaux@adelaide.edu.au; derek.abbott@adelaide.edu.au).

Color versions of one or more of the figures in this communication are available online at http://ieeexplore.ieee.org.

Digital Object Identifier 10.1109/TAP.2016.2647719

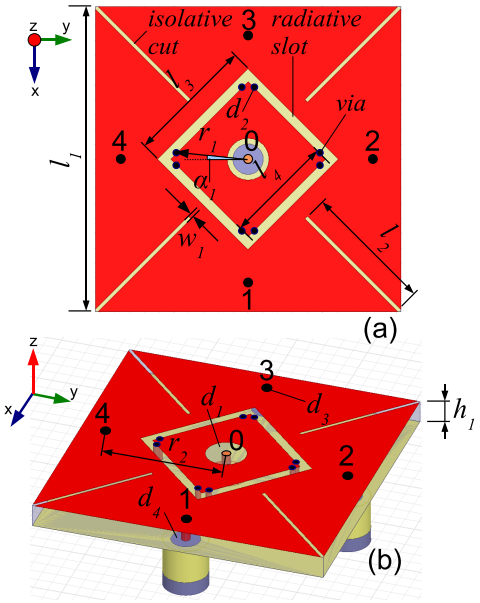

Fig. 1. Antenna design with port referencing. The design is symmetrical about the z-axis and includes a common radiative slot through in which polarization in three orthogonal directions is radiated. (a) Antenna topside view showing the square slot and the position of the eight monopole cavity grounding via connections and five coaxial probe feed connections, 0 to 4. Port 0 has topside clearance d_1 as a result of its mode of operation. In this communication, the coaxial probe feeds are replaced with five via pin connections inserted and soldered between the three-port feed backside and the antenna topside. (b) Additional dimension detailing of the antenna. The antenna backside is completely metallized, except for the five coaxial port ground clearances. Dielectric material is removed from Fig. 1(b) for convenience. Dimensions are explicitly described in Table I.

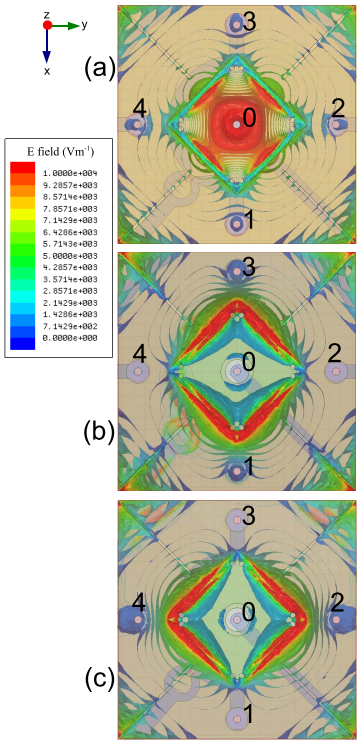

Fig. 2. Three fundamental modes of operation of the proposed antenna. Shown in this figure are simulated instantaneous electric field magnitudes, as seen from the antenna topside. (a) Magnetic current loop mode, or OLP radiation, excited by antenna port 0. (b) Degenerated broadside radiation, excited by differential feeding of antenna ports numbered 1 and 3. (c) Degenerated broadside radiation, excited by differential feeding of antenna ports numbered 2 and 4. Radiation of all three modes is via the common radiative slot.

2) *Orthogonal Broadside Modes:* The two orthogonal degenerated LP modes, shown in Fig. 2(b) and (c), are obtained by differential feeding on the opposite corners of the square slot [22]. A feeding network, described later in Section II-C, introduces differential feeding of opposite ports numbered 1 and 3, and 2 and 4 of the square slot, as numbered in Fig. 1. This feeding arrangement provides the two orthogonal broadside modes, radiating from the common square slot with polarizations parallel to the antenna surface.
3) *Multimode Radiative Square Slot:* Combining the previously described modes through appropriate feeding of the square slot, the antenna becomes effectively a three-port device. The actual feeds are realized through coaxial probes fed in five positions, numbered in Fig. 1, from the backside of the substrate. Unlike uni and dual-polarized designs that do not need to consider the implications of a slight break of symmetry about the center of the design, the design presented in this communication requires a high grade of mode symmetry to achieve high isolation between polarizations. This is because the coupling between a perfect symmetrical mode and a perfect antisymmetrical mode with the same phase center is theoretically zero.
4) *Scalability:* This design provides scalability through symmetry, while low mutual coupling is assured through the differential feeding mechanism, which is also scalable using the method demonstrated in this communication.

In summary, port 0 refers to the OLP port at the antenna center, providing the magnetic current loop mode of operation, while ports 1 to 4 are labeled sequentially about the outer portion of the antenna, providing the two orthogonal degenerated broadside modes of operation when fed differentially pairwise. All five ports are designed using a 50-Ω characteristic, and so the antenna may be integrated with a variety of feeding networks, or be used as a standalone device with high frequency digital inputs.

B. Specific Antenna Design

For the demonstration of the concept, a specific realization of the antenna is designed for operation at 5.89 GHz, in the allocated dedicated short range communications spectrum. The antenna is designed using the HFSS simulation tool. It is manufactured using Rogers RT Duroid 5880 material, with a relative permittivity of 2.20, thickness h_1 of 3.18 mm, and is cladded with industry standard 17 μm of copper on either side. Optimized dimensions are given in Table I.

1) The design starts with the creation of a planar monopole, as shown in [21]. An initial slot side length is one half of a guided wavelength, later optimized as l_3.
2) An initial ground via radial distance, establishing the cavity for magnetic current loop mode operation, is one quarter of a guided wavelength, or 9.1 mm, later optimized as r_1.
3) Feeds to excite the square slot in the broadside modes are then added. To provide high isolation between operation modes, an initial radial distance of one half of a guided wavelength, or 18.25 mm, is used between port 0 and ports 1 to 4.
4) To improve adjacent port isolation, in the instance of a non-differential feeding technique being used, four inward diagonal isolator slots are etched on the metallization of the antenna upper surface. With the design optimized, including the uniform radiative slot width, triorthogonal overlapping frequency responses at the design frequency of the two orthogonal

TABLE I
ANTENNA DIMENSIONS

Reference	Dimension
l_1 (antenna side length)	41.20 mm
h_1 (antenna substrate height)	3.18 mm
l_2 (isolator cut length)	18.00 mm
w_1 (isolator cut width)	0.50 mm
l_3 (common slot length)	17.26 mm
l_4 (OLP port cavity length)	14.76 mm
d_1 (OLP port pin clearance)	2.84 mm ⊘
r_1 (via radial distance)	9.70 mm
α_1 (via angle offset)	4.50°
d_2 (via diameter)	0.85 mm ⊘
r_2 (port pin radial distance)	17.19 mm
d_3 (port pin hole diameter)	1.50 mm ⊘
d_4 (copper ground clearance)	4.10 mm ⊘

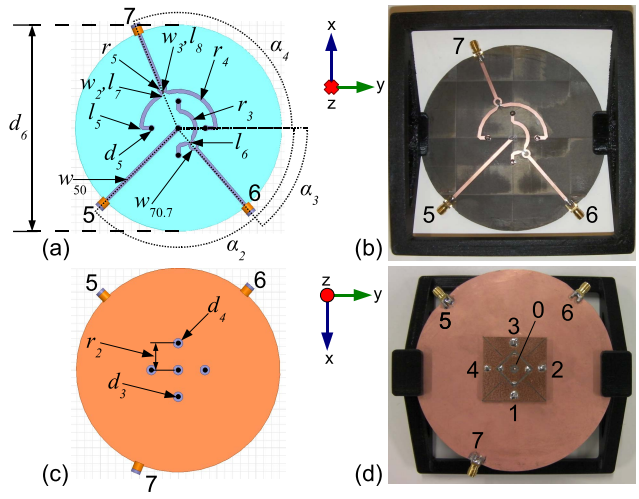

Fig. 3. Triorthogonal feed design with port referencing. Refer to Tables I and II for reference descriptions. (a) Virtual triorthogonal feed backside view showing feed line detail. (b) Manufactured feed backside view. (c) Virtual feed ground or topside view showing copper ground clearances. These clearances align with those on the antenna backside, allowing for five-port via pin connections to be inserted and soldered between feed backside and antenna topside. (d) Manufactured feed with antenna mounted for triorthogonal operation. System operation is performed with the antenna facing skyward, in the positive z-axis.

degenerated broadside modes and the magnetic current loop mode are achieved.

5) Port matching of the OLP port to a 50-Ω characteristic impedance is achieved with an annular gap around the center OLP port pin 0 on the antenna topside [21]. In effect, the capacitance of the annular gap compensates the inductive nature of the cavity coaxial feed. The LP port pins numbered 1 to 4 are matched to a 50-Ω characteristic impedance by varying their common radial distance r_2 from the antenna center.

C. Feed Arrangement for Triorthogonal Operation

Differential feed designs are able to provide polarization purity through opposing port field cancelation [17], and hence reduce port coupling, as well as provide phase centering [22]–[29]. It will be shown that this is an appropriate feeding technique if a third polarization is to be included in a phase-centered triorthogonal design.

Fig. 3 shows virtual and manufactured versions of a feed providing triorthogonal operation. Dimensions are given in Table II. The feed copper ground clearances and port pin holes, in Fig. 3(c), align with those of the antenna. Operation through antenna port excitation is achieved by five-port via pins inserted and soldered through the port pin hole between feed backside and antenna topside. Port pins 1–4 provide a means of attachment for the antenna to the feed, which is suitable for testing purposes.

TABLE II
FEED DIMENSIONS

Reference	Dimension
w_{50} (50 Ω line width)	2.43 mm
$w_{70.7}$ (70.7 Ω line width)	1.38 mm
α_2 (ports 5 and 8 connector angle)	135.00°
α_3 (port 6 connector angle)	48.50°
α_4 (port 7 connector angle)	113.00°
r_3 (polarization in x direction feed line center radius)	10.80 mm
r_4 (polarization in y direction feed line center radius)	23.60 mm
r_5 (Wilkinson divider internal radius)	1.70 mm
d_5 (port pin connection diameter)	3.70 mm ⊘
l_5 (external champfer length)	2.72 mm
l_6 (resistor gap)	0.50 mm
w_2,l_7 (outer Wilkinson divider champfer ; width, depth)	5.36 mm, 2.60 mm
w_3,l_8 (inner Wilkinson divider champfer ; width, depth)	1.40 mm, 1.00 mm
d_6 (feed diameter)	130.00 mm ⊘
α_5 (port 9 connector angle)	30.00°
r_6 (CP feed line central radius)	39.70 mm

This feeding circuit is manufactured using Rogers RT Duroid 5880 material, with a thickness of 0.787 mm. Both feeds are based on a 50-Ω characteristic impedance. Opposing ports are fed differentially, i.e., in antiphase. This creates field cancelation, by exciting an antisymmetric mode with a null, at the antenna center and so provides high isolation between the OLP and LP modes. Wilkinson power dividers with 100-Ω resistors are placed at power splitting junctions to improve isolation between ports in the LP feed arms [27], [30]. This improves input return losses through the reduction of unwanted voltage reflections.

For the triorthogonal system, the OLP feed to antenna port 0 is designated as port 5, while port 6 excites antenna ports 1 and 3 to provide polarization in the x-direction. Port 7 excites antenna ports 2 and 4 to provide polarization in the y-direction.

III. RESULTS

The antenna backside and feeding circuit topside ground planes are brought together and connector holes aligned for port pin connections. We maintain a 50-Ω characteristic impedance through copper ground clearances of diameter d_4 at each connection point. Connections between feed and antenna are then soldered, resulting in a three-port triorthogonal system. For measurement, the system is supported by a 3-D printed stand, shown in Fig. 3(b) and (d). The feed is larger than would be the case in an integrated solution in order to provide the ease of rotation in measurement. The microstrip arrangement for feeding port 5 provides a convenient planar feeding mechanism that avoids any potential coupling effects with port 6.

For the ease of understanding, we have determined three polarizations: x, y, and z, according to the feeding alignments shown in Fig. 3. The third Ludwig definition of cross polarization is used to determine LP performance [31]. We provide figures that also demonstrate out-of-band performance over the 4–8-GHz frequency range. Fig. 4(a) and (b) shows the simulated and measured reflection coefficient of the OLP and broadside LP feeds. The measured resonance of S_{55} at 6.9 GHz is an effect of impedance matching Z_{55}, which

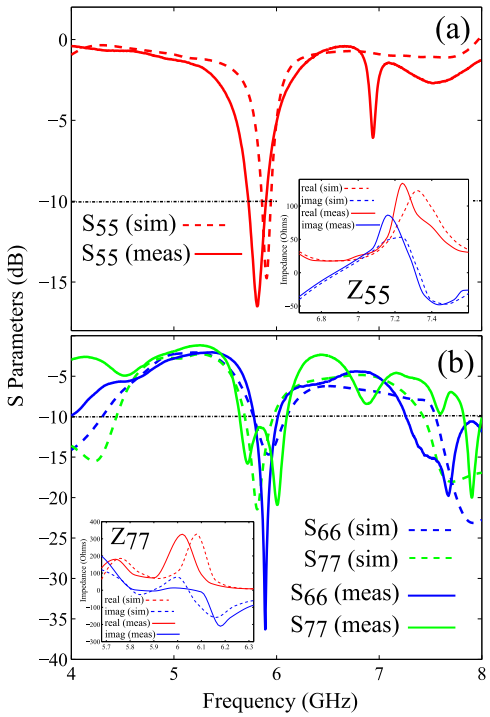

Fig. 4. Simulated and measured port reflection coefficients of the LP system. (a) OLP feed (S_{55}). (b) Broadside LP feeds (S_{66} and S_{77}). A reflection coefficient specification line of −10 dB is shown for convenience. Insets: impedance matching causes the effects observed on measured S_{55} at 6.9 GHz and on measured S_{77} at 5.7–6.2 GHz.

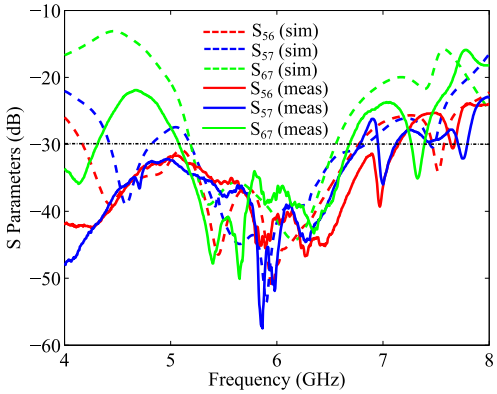

Fig. 5. Simulated and measured port isolation coefficients of the LP system: S_{56}, S_{57}, and S_{67}. An isolation coefficient specification line of 30 dB is shown for convenience.

is shown in Fig. 4(a) (inset). A resonance is defined as where the imaginary component of impedance crosses the zero impedance line. The measured double resonance of S_{77} at 5.7–6.2 GHz is an effect of impedance matching Z_{77}, which is shown in Fig. 4(b) (inset). Fig. 5 shows port isolation characteristics. The OLP resonance is measured as shifted downward in frequency to 5.81 GHz, or by an order of 1%, in comparison to that simulated. This phenomenon has been noted in the previous work using the same design materials [21], and is likely due to tolerances in a nonindustrial manufacturing process. The OLP impedance bandwidth, defined as a reflection coefficient less than −10 dB, is measured as 185 MHz (5.72–5.91 GHz), or 3.18%.

Both LP polarizations, in the x- and y-directions, resonate at the design frequency, although polarization in the y-direction, fed by the outer feed radius via port 7, possesses a wider bandwidth of 495 MHz (5.64–6.13 GHz), or 8.41%, than polarization in the x-direction,

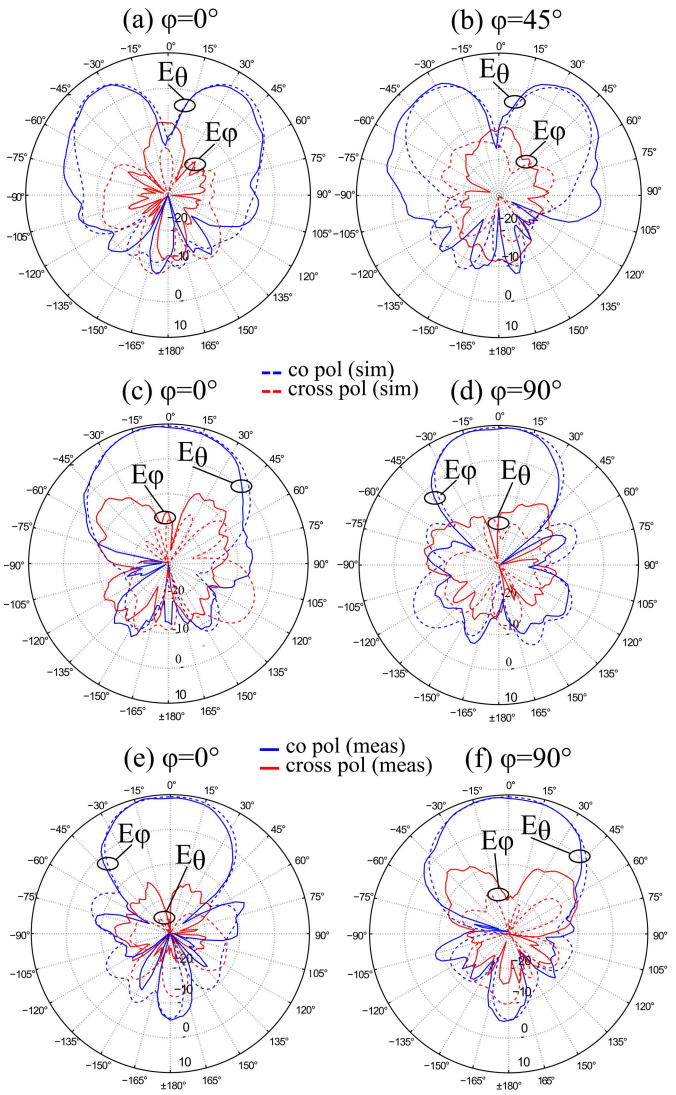

Fig. 6. (a) and (b) OLP radiation characteristic achieved via excitation of port 5 of the LP feed and antenna combination. (c) and (d) Excitation of port 6 provides an LP radiation characteristic in the x-direction. (e) and (f) Excitation of port 7 provides an LP radiation characteristic in the y-direction. Asymmetry in patterns results from the feeding interface and the imperfection of the measurement environment.

fed by the inner feed radius via port 6, with bandwidth of 280 MHz (5.77–6.01 GHz), or 4.74%. The difference is observed in both simulation and measurement, and is an effect of the short line length to the inner feed pin exciting antenna port 3. Isolation of no less than 30 dB is measured from 5.10–6.70 GHz. The isolative effect of the Wilkinson power dividers is observed through S_{66} and S_{77} and the reflection coefficients of feed lines requiring isolation between fed antenna ports 1 and 3, and 2 and 4, respectively. The isolative effect of driving opposing ports in antiphase to create degenerated broadside mode field cancelation, or a null, at the antenna phase center, where the OLP resonator is situated, is observed through S_{56} and S_{57}. Isolation between port 0, and antenna ports 1 and 3, and 2 and 4, driven by feed ports 5–7, respectively, is theoretically infinite. In reality, an isolation S_{57} up to 57 dB was achieved. The smallest overlapping triorthogonal operational bandwidth is measured as 135 MHz (5.77–5.91 GHz), or 2.3%.

Fig. 6 provides OLP and LP gain profiles. Fig. 6(a) and (b) shows simulated and measured results for OLP radiation, excited through

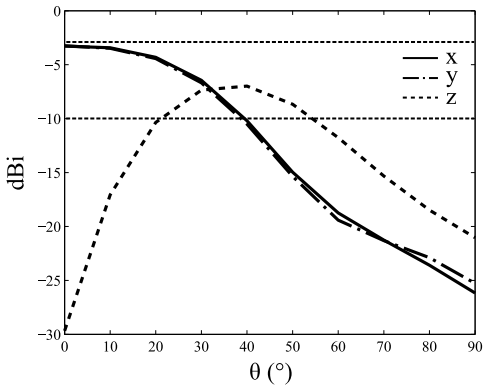

Fig. 7. MEGs for the three orthogonal polarizations in dBi as a function of θ from the zenith position, orthogonal to the antenna radiating surface, using simulated 3-D radiation patterns and radiation efficiency. MEG limits of -3 and -10 dBi are included for the ease of data -3 and -10 dBi are included for the ease of data interpretation.

TABLE III

MEGs FOR THE THREE ORTHOGONAL POLARIZATIONS IN dBi AS A FUNCTION OF SOLID ANGLE SUBTENDED FROM THE ZENITH POSITION, ORTHOGONAL TO THE ANTENNA RADIATING SURFACE (FROM SIMULATED 3-D RADIATION PATTERNS AND RADIATION EFFICIENCY)

	0°-30°	0°-60°	0°-90°	30°-60°	60°-90°
x	-4.19	-6.24	-7.75	-10.38	-21.61
y	-4.28	-6.35	-7.86	-10.65	-21.71
z	-11.29	-10.00	-11.24	-8.34	-15.30

port 5, at azimuthal angles ϕ of 0° and 45°, respectively. The OLP radiation pattern confirms the operation as a magnetic current loop. It is simulated and measured as conical, with absolute peak realized gain of 6.4 dB at $\theta = \pm 35°$. Antenna LP diversity in either the x- or y-direction is realized by differentially exciting port pair 1 and 3 through port 6, or 2 and 4 through port 7, respectively. This leads to the excitation of either of the two orthogonal degenerated broadside modes, and radiation with peak gain in the z-direction.

Two commonly used criteria, i.e., the mean effective gain (MEG) [32], and the envelope correlation (ECC) [33], are utilized to evaluate the antenna diversity performance. Both MEG and ECC metrics are calculated using spherical integration functions of the 3-D far-field antenna patterns. For MEG, we base calculations on [32, eq. (1)]. At the design frequency of 5.89 GHz, we report the MEGs as a function of θ in Fig. 7, and as a function of solid angle in Table III in a line-of-sight channel. We measure the values of θ and solid angles from the antenna zenith, orthogonal to the antenna radiating surface. An ideal MEG will be -3 dBi in the case of 100% radiation efficiency, a cross polarization ratio (XPR) of 0 dB at the transmitter and receiver, and it should be above -10 dBi for a practical antenna. According to the port isolation coefficients of Fig. 5, we introduce polarization coupling coefficients at the receiver into the diversity model in [34], providing an upper bound on cross polarization discrimination values at the receiver. At the transmitter, we are only concerned with the two polarizations that are aligned with the receiver at the field of view center in the diversity model in [34]. We model an XPR of 0 dB between these polarizations at the transmitter through polarization coupling coefficients of zero magnitude. As such, simulated data are output as a function of the triorthogonal receive antenna uniquely. Simulated antenna radiation efficiency is above 94%, with a worst case measured radiation efficiency of 86%. Fig. 7 highlights that the MEGs of polarizations x and y are near optimal at -3.28 and -3.25 dBi, respectively, when the antenna radiating surface is perfectly aligned with the transmitter. Polarization z provides an MEG that is optimal at 40°, but that does not reach the optimal values of x and y. It does, however, provide a higher MEG than x and y for the values of $\theta \geq 32°$. In effect, polarization z extends the angular range of the antenna, in a practical sense as defined by a lower MEG limit of -10 dBi, from θ=40° to 54°. The omnidirectional radiation pattern associated with polarization z is slightly conical in nature, as observed in Fig. 6(a) and (b), and this is due to the compact sizing of the ground plane. For an extended ground plane, such as that of an external metallic skin of a vehicular mode of transport (i.e., car and bus), it is suggested that the slightly conical radiation pattern would approach that of a monopole, providing more gain at higher values of θ, and thus extend the practical angular range of the antenna.

TABLE IV

ENVELOPE CORRELATION COEFFICIENTS (FROM SIMULATED 3-D RADIATION PATTERNS)

Frequency	Polarizations	ECC
5.77 GHz	xz	2e-02
	yz	1e-03
	xy	3e-02
5.89 GHz	xz	6.6e-04
	yz	6.9e-04
	xy	1e-03
5.91 GHz	xz	1e-02
	yz	1e-03
	xy	3e-02

We also report the ECCs shown in Table IV over the antenna upper radiating hemisphere. An upper threshold of 0.5 is commonly held as acceptable, while a value of 0 would suggest no correlation between polarizations. According to [35, eq. (1)], the ECC may be calculated from the simulated far-field radiation patterns. The proposed antenna demonstrates low correlation between all three polarizations at the center, and at the band edges, of the overlapping triorthogonal bandwidth. The antisymmetric–symmetric nature of distributed electric fields between x and z, and y and z polarizations, and the symmetry of the physical design, provides near zero correlation. The ECC between x and y polarizations is slightly higher but still low due to the orthogonal polarization of the modes involved. The introduction of the omnidirectional pattern improves worst case diversity performance, which commonly occurs at $\phi = 45°$. A cross correlation of 0.3323 is calculated between broadside modes and the omnidirectional mode at (45° and 45°), this radiating direction being furthest from orthogonality.

IV. DISCUSSION

A planar slot antenna operating at 5.9 GHz and providing tri-orthogonal diversity operation is proposed in this communication. Triorthogonal polarization operation from a shared radiative slot on the top surface of the design is simulated, and subsequently confirmed through measurement. Radiation from the three modes of operation, two orthogonal degenerated broadside modes, and a magnetic current loop mode, is measured. The antenna provides 6.4 dB of OLP gain and 9.4 dB of maximum LP gain at the design frequency, and operates with a minimum measured triorthogonal overlapping impedance bandwidth of 2.3% (5.77–5.91 GHz).

Isolation of no lower than 35 dB was measured between the three modes in the frequency band of operation, due to field cancelation of the two orthogonal degenerated broadside modes at the antenna center, as a result of differential port feeding.

This discussion demonstrates a general proof-of-concept. As possible extension to this communication, the antenna radiation pattern may be controlled in three orthogonal axes by combining feeding excitations to each of the antenna ports with varying relative phases and amplitudes. Optimizing performance metrics for given applications remains an open question for the future work.

REFERENCES

[1] S. L. S. Yang, K. M. Luk, H. W. Lai, A. A. Kishk, and K. F. Lee, "A dual-polarized antenna with pattern diversity," *IEEE Antennas Propag. Mag.*, vol. 50, no. 6, pp. 71–79, Dec. 2008.

[2] A. Chebihi, C. Luxey, A. Diallo, P. L. Thuc, and R. Staraj, "A novel isolation technique for closely spaced PIFAs for UMTS mobile phones," *IEEE Antennas Wireless Propag. Lett.*, vol. 7, pp. 665–668, Sep. 2008.

[3] A. Diallo, C. Luxey, P. Le Thuc, R. Staraj, and G. Kossiavas, "Study and reduction of the mutual coupling between two mobile phone PIFAs operating in the DCS1800 and UMTS bands," *IEEE Trans. Antennas Propag.*, vol. 54, no. 11, pp. 3063–3074, Nov. 2006.

[4] V. Erceg, H. Sampath, and S. Catreux-Erceg, "Dual-polarization versus single-polarization MIMO channel measurement results and modeling," *IEEE Trans. Wireless Commun.*, vol. 5, no. 1, pp. 28–33, Jan. 2006.

[5] R. U. Nabar, H. Bolcskei, V. Erceg, D. Gesbert, and A. J. Paulraj, "Performance of multiantenna signaling techniques in the presence of polarization diversity," *IEEE Trans. Signal Process.*, vol. 50, no. 10, pp. 2553–2562, Oct. 2002.

[6] Y. Li, Z. Zhang, J. Zheng, and Z. Feng, "Compact azimuthal omni-directional dual-polarized antenna using highly isolated colocated slots," *IEEE Trans. Antennas Propag.*, vol. 60, no. 9, pp. 4037–4045, Sep. 2012.

[7] R. R. Ramirez and F. D. Flaviis, "A mutual coupling study of linear and circular polarized microstrip antennas for diversity wireless systems," *IEEE Trans. Antennas Propag.*, vol. 51, no. 2, pp. 238–248, Feb. 2003.

[8] M. R. Andrews, P. P. Mitra, and R. de Carvalho, "Tripling the capacity of wireless communications using electromagnetic polarization," *Nature*, vol. 409, pp. 316–318, Oct. 2001.

[9] M. C. Mtumbuka, W. Q. Malik, C. J. Stevens, and D. J. Edwards, "A tri-polarized ultra-wideband MIMO system," in *Proc. IEEE Symp. Adv. Wired Wireless Commun.*, Apr. 2005, pp. 98–101.

[10] C. Y. Chiu, J. B. Yan, and R. D. Murch, "Compact three-port orthogonally polarized MIMO antennas," *IEEE Antennas Wireless Propag. Lett.*, vol. 6, pp. 619–622, Dec. 2007.

[11] G. Yan, Z. Du, and K. Gong, "A compact orthogonal tripolarized multiantenna with low mutual coupling for MIMO channel measurements," *Microw. Opt. Technol. Lett.*, vol. 48, no. 7, pp. 1358–1362, 2006.

[12] M. C. Mtumbuka and D. J. Edwards, "Investigation of tri-polarised MIMO technique," *Electron. Lett.*, vol. 41, no. 3, pp. 137–138, Feb. 2005.

[13] J. X. Yun and R. G. Vaughan, "Slot MIMO cube," in *Proc. IEEE Antennas Propag. Soc. Int. Symp. (APSURSI)*, Sep. 2010, pp. 1–4.

[14] C. Y. Chiu, J. B. Yan, R. D. Murch, J. X. Yun, and R. G. Vaughan, "Design and implementation of a compact 6-port antenna," *IEEE Antennas Wireless Propag. Lett.*, vol. 8, pp. 767–770, Sep. 2009.

[15] B. N. Getu and J. B. Andersen, "The MIMO cube—A compact MIMO antenna," *IEEE Trans. Wireless Commun.*, vol. 4, no. 3, pp. 1136–1141, May 2005.

[16] B. N. Getu and R. Janaswamy, "The effect of mutual coupling on the capacity of the MIMO cube," *IEEE Antennas Wireless Propag. Lett.*, vol. 4, pp. 240–244, Jul. 2005.

[17] L. Zou and C. Fumeaux, "A cross-shaped dielectric resonator antenna for multifunction and polarization diversity applications," *IEEE Antennas Wireless Propag. Lett.*, vol. 10, pp. 742–745, Jul. 2011.

[18] H. Zhong, Z. Zhang, W. Chen, Z. Feng, and M. Iskander, "A tripolarization antenna fed by proximity coupling and probe," *IEEE Antennas Wireless Propag. Lett.*, vol. 8, pp. 465–467, Oct. 2009.

[19] X. Gao, H. Zhong, Z. Zhang, Z. Feng, and M. F. Iskander, "Low-profile planar tripolarization antenna for WLAN communications," *IEEE Antennas Wireless Propag. Lett.*, vol. 9, pp. 83–86, Feb. 2010.

[20] K.-F. Tong, H.-J. Tang, A. Al-Armaghany, and W. Hong, "Low-profile orthogonally tripolarized antennas," *IEEE Antennas Wireless Propag. Lett.*, vol. 12, pp. 876–879, Feb. 2013.

[21] T. Kaufmann and C. Fumeaux, "Low-profile magnetic loop monopole antenna based on a square substrate-integrated cavity," *Int. J. Antennas Propag.*, vol. 2015, Jun. 2015, Art. no. 694385, doi: 10.1155/2015/694385.

[22] R. C. Paryani, P. F. Wahid, and N. Behdad, "A wideband, dual-polarized, substrate-integrated cavity-backed slot antenna," *IEEE Antennas Wireless Propag. Lett.*, vol. 9, pp. 645–648, Jul. 2010.

[23] H. Huang, Y. Liu, and S. Gong, "A novel uniplanar differentially-fed UWB polarization diversity antenna with dual notch bands," *IEEE Antennas Wireless Propag. Lett.*, vol. 14, no. 3, pp. 563–566, Apr. 2015.

[24] G. Adamiuk, W. Wiesbeck, and T. Zwick, "Differential feeding as a concept for the realization of broadband dual-polarized antennas with very high polarization purity," in *Proc. IEEE Antennas Propag. Soc. Int. Symp. (APSURSI)*, Jun. 2009, pp. 1–4.

[25] G. Adamiuk, S. Beer, W. Wiesbeck, and T. Zwick, "Dual-orthogonal polarized antenna for UWB-IR technology," *IEEE Antennas Wireless Propag. Lett.*, vol. 8, pp. 981–984, Oct. 2009.

[26] F. Zhu *et al.*, "Ultra-wideband dual-polarized patch antenna with four capacitively coupled feeds," *IEEE Trans. Antennas Propag.*, vol. 62, no. 5, pp. 2440–2449, May 2014.

[27] T.-W. Chiou and K.-L. Wong, "Broad-band dual-polarized single microstrip patch antenna with high isolation and low cross polarization," *IEEE Trans. Antennas Propag.*, vol. 50, no. 3, pp. 399–401, Mar. 2002.

[28] Q. Xue, S. W. Liao, and J. H. Xu, "A differentially-driven dual-polarized magneto-electric dipole antenna," *IEEE Trans. Antennas Propag.*, vol. 61, no. 1, pp. 425–430, Jan. 2013.

[29] M. Li and K.-M. Luk, "A differential-fed magneto-electric dipole antenna for UWB applications," in *Proc. Asia–Pacific Microw. Conf. (APMC)*, Dec. 2011, pp. 1953–1956.

[30] D. Pozar, *Microwave Engineering*, 4th ed. Hoboken, NJ, USA: Wiley, 2011.

[31] A. Ludwig, "The definition of cross polarization," *IEEE Trans. Antennas Propag.*, vol. 21, no. 1, pp. 116–119, Jan. 1973.

[32] T. Taga, "Analysis for mean effective gain of mobile antennas in land mobile radio environments," *IEEE Trans. Veh. Technol.*, vol. 39, no. 2, pp. 117–131, May 1990.

[33] T. W. C. Brown, S. R. Saunders, S. Stavrou, and M. Fiacco, "Characterization of polarization diversity at the mobile," *IEEE Trans. Veh. Technol.*, vol. 56, no. 5, pp. 2440–2447, Sep. 2007.

[34] N. P. Lawrence, B. W.-H. Ng, H. J. Hansen, and D. Abbott, "Analysis of millimetre-wave polarization diverse multiple-input multiple-output capacity," *Roy. Soc. Open Sci.*, vol. 2, no. 12, p. 150322, Dec. 2015.

[35] S. M. Mikki and Y. M. M. Antar, "On cross correlation in antenna arrays with applications to spatial diversity and MIMO systems," *IEEE Trans. Antennas Propag.*, vol. 63, no. 4, pp. 1798–1810, Apr. 2015.